

Dynamic Stall

Pereira, Ricardo Santos

DOI

[10.1007/978-3-030-31307-4_14](https://doi.org/10.1007/978-3-030-31307-4_14)

Publication date

2022

Document Version

Final published version

Published in

Handbook of Wind Energy Aerodynamics

Citation (APA)

Pereira, R. S. (2022). Dynamic Stall. In *Handbook of Wind Energy Aerodynamics: With 678 Figures and 33 Tables* (pp. 331-351). Springer. https://doi.org/10.1007/978-3-030-31307-4_14

Important note

To cite this publication, please use the final published version (if applicable). Please check the document version above.

Copyright

Other than for strictly personal use, it is not permitted to download, forward or distribute the text or part of it, without the consent of the author(s) and/or copyright holder(s), unless the work is under an open content license such as Creative Commons.

Takedown policy

Please contact us and provide details if you believe this document breaches copyrights. We will remove access to the work immediately and investigate your claim.

Green Open Access added to TU Delft Institutional Repository

'You share, we take care!' - Taverne project

<https://www.openaccess.nl/en/you-share-we-take-care>

Otherwise as indicated in the copyright section: the publisher is the copyright holder of this work and the author uses the Dutch legislation to make this work public.



Dynamic Stall

10

Ricardo Santos Pereira

Contents

Introduction	332
Physical Phenomenon Description	333
Occurrence of Dynamic Stall	334
Influence of Operational Parameters on Dynamic Stall Behaviour	336
Dynamic Stall on Wind Energy Machines	338
Dynamic Stall on HAWT	338
Dynamic Stall on VAWT	340
Experimental Data on Dynamic Stall	341
Dynamic Stall Modelling	342
Beddoes-Leishman Type of Dynamic Stall Modelling	343
Modelling Dynamic Stall in Wind Energy Machines	347
Cross-References	348
References	349

Abstract

Dynamic stall is a complex fluid dynamics problem that occurs on an airfoil during rapid, transient motion in which the angle of attack goes beyond the static stall angle. Since the instantaneous sectional aerodynamic loads may surpass the static values, dynamic stall events often dictate the operational load range in several systems, including wind energy machines. Typically the phenomenon of dynamic stall is modelled using semi-empirical or the so-called engineering approaches, derived from 2D wind tunnel tests. However, extrapolation to wind energy machines' behaviour must be done carefully as real conditions of DS occurrence arise as a combination of complex, interacting phenomena,

R. Santos Pereira (✉)
Faculty of Aerospace, Delft University of Technology, Delft, The Netherlands
e-mail: asimov1984@gmail.com

including 3D aerodynamic features (e.g. due to yaw misalignment and rotational augmentation) and also blade structural vibrations.

Keywords

Dynamic stall · Unsteady aerodynamics · Airfoil aerodynamics

Introduction

Generally speaking, dynamic stall (DS) is an unsteady aerodynamic phenomenon which occurs when the angle of attack (AOA) experienced by an airfoil fluctuates rapidly beyond the (static) stall AOA or, in other words, when the airfoil stalls in a dynamic fashion, with a markedly transient behaviour. During dynamic stall, the instantaneous aerodynamic sectional forces often exceed the static values, and thus DS events may determine the operational load envelope of many aerodynamic systems. Though an increased lift in DS conditions may be beneficial to bumble bees (Magnan 1934) as it enables these insects to fly with very small wings, increased load fluctuations are particularly harmful for rotary machines, as the cyclic loading causes fatigue damage to rotor blades of helicopters (Leishman 2006) and wind turbines (Leishman 2002).

This section describes the dynamic stall phenomenon as well as its occurrence on wind energy (WE) machines. Experimental data is shown and finally a discussion on the modelling of dynamic stall is provided.

Before we proceed to further characterize dynamic stall, it is important to note that in the context of WE, different unsteady aerodynamic time scales are relevant. We can estimate the characteristic time scale by considering the pertinent velocity and length scales.

The aerodynamic load transients occurring over the entire turbine rotor, associated with the wake aerodynamics, have a time scale in the order of $\tau = D/U$, where D stands for the diameter of the rotor and U represents wind velocity. Such unsteady aerodynamic phenomena can thus be considered ‘slow’; for modern MW size machines, it is clear the correspondent time scales are in the order of a few seconds $O(10^0)$ s. A typical example of the so-called *dynamic inflow* is a sudden blade pitch angle change, in which an equilibrium between wake induction and rotor loads is only achieved several seconds after the pitch adjustment.

By contrast, we should note the aerodynamic transient phenomena taking place at a blade section level have a characteristic time scale $\tau = c/V$, where c is the local chord and V stands for effective velocity. For outboard sections of modern MW size machines, this corresponds to time scales of a few hundredths of a second $O(10^{-2})$ s and thus corresponds to ‘fast’ phenomena. In this context, *Dynamic Stall* may be classified as a ‘fast’ WE unsteady aerodynamic effect. In practice such events often occur on wind energy machines due to atmospheric turbulence and blade vibrations, as discussed later in this chapter.

Although in reality rotor-scale and blade-scale aerodynamic unsteady effects might interplay, in terms of physical modelling it is common to separate these phenomena, because of the different time scales.

Physical Phenomenon Description

When an airfoil experiences an oscillation in AOA in which it goes beyond the static stall angle, DS may take place. This means several subsequent phenomena occur, with a rather complex overall behaviour of the airfoil loading, and yielding instantaneous aerodynamic forces very different from those obtained in quasi-static regimes. Dynamic stall is characterized by a vortex build-up near the leading edge of the airfoil as the AOA increases, causing a lift overshoot. Subsequently there is an abrupt decrease in the normal force C_n when the accumulated vortex is convected downstream of the airfoil as the AOA decreases, together with very large variations in pitching moment C_m due to centre of pressure movements. It is useful to divide the DS phenomenon in five stages (Leishman 2006) to better grasp the sequence of events, as illustrated in Fig. 1.

As the AOA increases rapidly in stage 1, there is a reduction in adverse pressure gradients along the chord, compared to the quasi-steady case for the same incidence, and the onset of separation is postponed. Further augmenting the AOA, and as the separation point approaches the leading edge, there is an accumulation of vorticity in that region of the airfoil, i.e. the leading edge vortex becomes stronger, bringing us to stage 2. At some point, the vortex will be released from the leading edge and swept downstream over the chord, causing an aft movement of the centre of pressure and thus a large nose-down pitching moment, usually referred to as moment stall. It is noted however that as long as the vortex structure is over the airfoil upper surface, it will provide additional lift.

Stage 3 is characterized by a sudden break in C_l , which happens at a larger AOA than the abrupt pitching moment decrease. In other words, the moment stall will occur at the onset of vortex shedding, while the lift stall will happen only when the vortex passes into the airfoil wake. Afterwards the flow on the upper surface becomes fully separated, as the vortex passes the airfoil trailing edge, here denoted by stage 4. Subsequently, reattachment of the flow is significantly delayed, and full reattachment is postponed to configurations in which the airfoil is well below the static stall angle, corresponding to stage 5.

It is noted the phenomenological description provided here is somewhat generic. Though the overall physical processes follow the sequence described, it is possible to divide DS events into different stages (Sheng et al. 2006), and the actual aerodynamic forces' variation will depend on the specific airfoil geometry and forcing conditions, as discussed below.

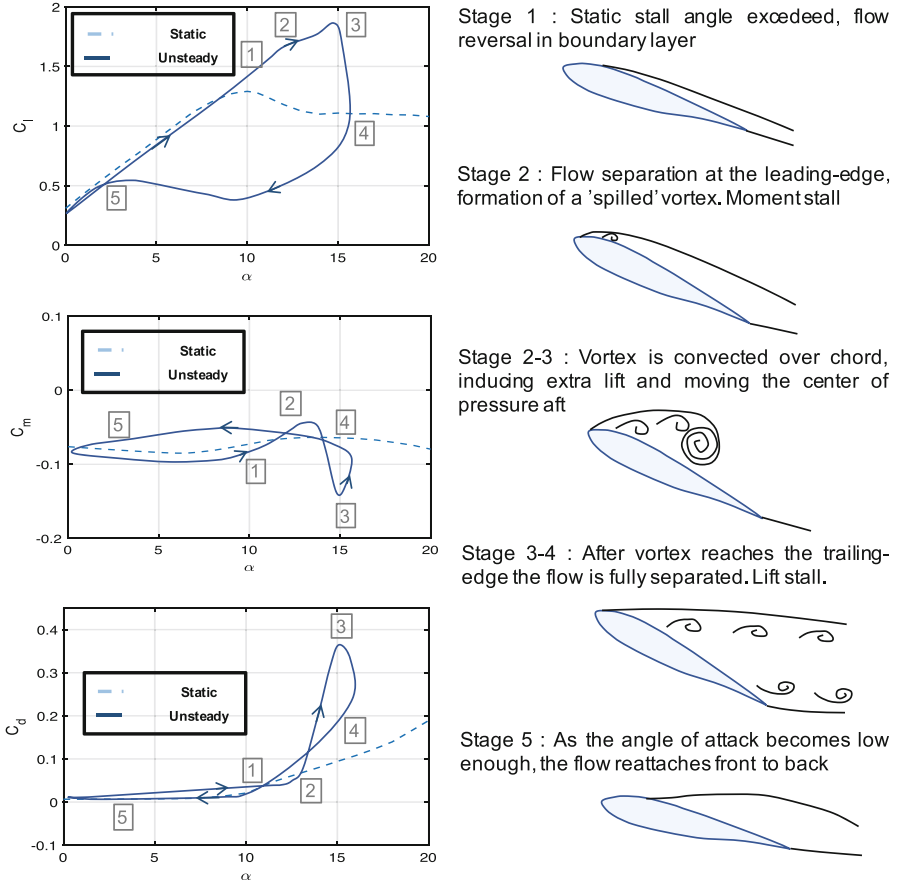


Fig. 1 Illustration of dynamic stall stages, following Leishman (2006)

Occurrence of Dynamic Stall

As described in the previous subsection, for dynamic stall to occur the experienced conditions must be **1** *Dynamic*, or unsteady, i.e. fluctuations in AOA, and **2** AOA ranging beyond the *airfoil (static) stall*. At this point some clarification is required.

1 – So far we mentioned DS occurring with ‘rapid’ variations in AOA; this is in practice usually assessed with the *reduced frequency* k , a non-dimensional parameter expressed with:

$$k = \frac{\omega \cdot c}{2V} \tag{1}$$

where ω is the excitation (angular) frequency, that is, the dominant frequency in the AOA time series $\alpha(t)$; symbol c denotes the length scale, i.e. the airfoil or blade section chord; and V expresses the local or effective velocity. The factor 2 in Expression 1 is introduced for historical reasons (Theodorsen 1935). From a physical perspective, the value of k expresses the degree of flow unsteadiness in a given aerodynamic system. According to Leishman (Leishman 2006) if $k > 0.2$, unsteady effects completely dominate the flow and if $k < 0.05$, the flow behaviour may be considered quasi-static. Though this ‘unsteadiness threshold’ has been adopted for helicopter aerodynamics, a smaller value $k < 0.02$ has been proposed by Snel (Snel 1997) for the onset of unsteady aerodynamic effects on WE machines.

An alternative way (Daley and Jumper 1984; Lorber and Carta 1987) to estimate the degree of flow unsteadiness is to consider the *reduced pitch rate* \dot{r} , defined analogously to the reduced frequency but using the AOA time derivative $\dot{\alpha}$ instead of the angular frequency. In case of a harmonic oscillation $\alpha(t) = A \sin(\omega t)$, the (maximum) reduced pitch rate is related with the reduced frequency by $\dot{r} = A k$, where A is the amplitude of the harmonic oscillation. According to Seto and Galbraith (Seto and Galbraith 1985), a reduced pitch rate of $\dot{r} = 0.01$ delimits the boundary of quasi-static and dynamic stall.

2 – Dynamic stall events occur when the experienced AOA is beyond the airfoil stall angle; unsteady aerodynamic effects are already noticeable at low incidence angles, while the flow is still attached to the airfoil surface. Such unsteady effects are associated with a lag in the adjustment of the pressure field to the varying AOA (Fung 1993) and also with the decaying influence of shed circulation as the vortical structures are convected downstream (Theodorsen 1935), often referred to as the *impulsive* and *circulatory* components, respectively (Leishman and Beddoes 1989). However, the behaviour in unsteady conditions at large AOA (i.e. when there is significant flow separation) is more relevant; the dynamic trailing edge separation and especially the leading edge vortex concentration and detachment leads to significant overshoots and drastic fluctuations in C_l , C_d and C_m , as mentioned in the previous section.

A number of criteria have been proposed for the onset of dynamic stall. From a physical perspective, and referring to Fig. 1, this corresponds to the influence of LE vorticity detachment and subsequent convection. In unsteady forcing, the exact conditions for LE vorticity detachment will depend on the instantaneous angle of attack and its temporal derivatives $\alpha(t)$, $\dot{\alpha}(t)$, etc.. Several researchers suggested different DS onset criteria, based both on local surface pressure and chord-integrated measurements. Previously suggested criteria include deviations in the (chord-integrated) normal and drag coefficients C_n or C_d , pitching moment break C_m , maximum value of chord force coefficient C_c and also the (local) C_p deviation at quarter-chord and the suction collapse of pressure at the leading edge LE. At this point it is noted the choice of the DS onset criterion is often associated with the specific modelling philosophy. Sheng et al. (Sheng et al. 2006, 2008) provide an excellent review of different criteria and argue the maximum C_c is probably the most suitable since it is obtained easily and is not significantly affected by local disturbances.

Selecting adequate DS onset criteria is also related with the specific airfoil shape. The geometry of the airfoil nose region determines (Timmer 2009) the AOA at which static LE separation occurs and thus also influences the LE vortex detachment under dynamic conditions. Because of the relatively large thickness to chord ratio, airfoils used in wind energy applications usually have a (static) soft stall, corresponding to a gradual movement of the separation point from the TE to the LE as the AOA increases (Bertagnolio 2001; Timmer and van Rooij 2003). As such, criteria based on pitching moment variations (Leishman and Beddoes 1989) are not always suitable for WE airfoils.

Influence of Operational Parameters on Dynamic Stall Behaviour

Naturally, different parameters will have a distinct influence on the instantaneous aerodynamic sectional forces occurring during DS events. The following trends hold for a 2D dynamic stall scenario:

Mean angle of attack $\bar{\alpha}$ – when considering an airfoil undergoing oscillatory motion, the average AOA dictates the degree of stall penetration in a cycle. If $\bar{\alpha}$ is small that is considerably smaller than the static stall angle, the airfoil experiences ‘light’ dynamic stall, meaning that the C_l vs α curve will resemble the ellipses (Theodorsen 1935) characteristic of attached flow and the oscillations in the pitching moment coefficient C_m will have small amplitude. By contrast, if the mean angle of attack is large (equal to the static stall angle or greater), the so-called ‘deep’ dynamic stall occurs. This is characterized by a large lift overshoot relatively to the static behaviour followed by an abrupt loss of lift and a significant nose-down pitching moment, indicative of large vortex shedding. As such, when $\bar{\alpha}$ is large, the aerodynamic force coefficients’ evolution over each cycle will have significant hysteresis.

Reduced Frequency k – since it may be interpreted as the degree of flow unsteadiness, as the reduced frequency increases the system will have less time to adapt to the variations in operating conditions. In practice, when the AOA is small, a larger reduced frequency will result in wider C_l vs α loops and thus more significant hysteresis. When the range of AOA over each cycle is large, and the instantaneous $\alpha(t)$ becomes larger than the static stall angle, increasing k delays the vortex shedding as well as flow reattachment. Further increasing the reduced frequency may even prevent flow separation from initiating at any point of the cycle (Leishman 2006).

Mach Number M – analogously to the static case, compressibility effects decrease the stall angle, thus meaning that for larger *Mach* numbers there will be more stall penetration and a larger amount of hysteresis in the whole cycle (Carr and Chandrasekhara 1996). If the local Mach number approaches the speed of sound, the onset of dynamic stall may involve a shock wave and there will be complex centre of pressure movements. It is noted however that for modern-day WE machines, compressibility effects are negligible under normal operation, as the blade section effective velocity is $V < 0.3M$.

Laminar-Turbulent Transition – the development of the boundary layer along the airfoil surface will depend on a number of factors, namely, the foil shape, local Re number and surface roughness. To emulate real operating conditions, particularly rotary machines with soiled blades, in (two-dimensional) airfoil sections’ wind tunnel tests, the flow is often tripped near the LE, i.e. transition is imposed. The effect that forced LE transition has on the DS behaviour however has received little attention in the past. Bousman (Bousman 2000) reports the maximum instantaneous lift when transition is imposed is generally smaller than for the free-transition case. As such the load amplitude when DS takes place is affected similarly to what happens in static conditions (Timmer and van Rooij 2003). However the load dynamics, specifically the lag on the unsteady loading with respect to the instantaneous AOA, seems to be relatively insensitive to (forced) LE transition.

Figure 2 shows 2D experimental results (National Renewable Energy Laboratories) at different reduced frequencies, for two airfoil sections. The instantaneous values of the (phase-averaged) sectional lift, drag and pitching moment are illustrated. The effect of k on the load cycle is clear, with increased hysteresis at higher reduced frequencies. As separation is delayed, the LE vortex is stronger at higher reduced frequencies, leading not only to increased lift but also to a sharper lift stall, as shown in the $C_l(\alpha)$ loops. The effect of the airfoil geometry section is also clear; one observes virtually no moment break for the thicker airfoil, whereas for the

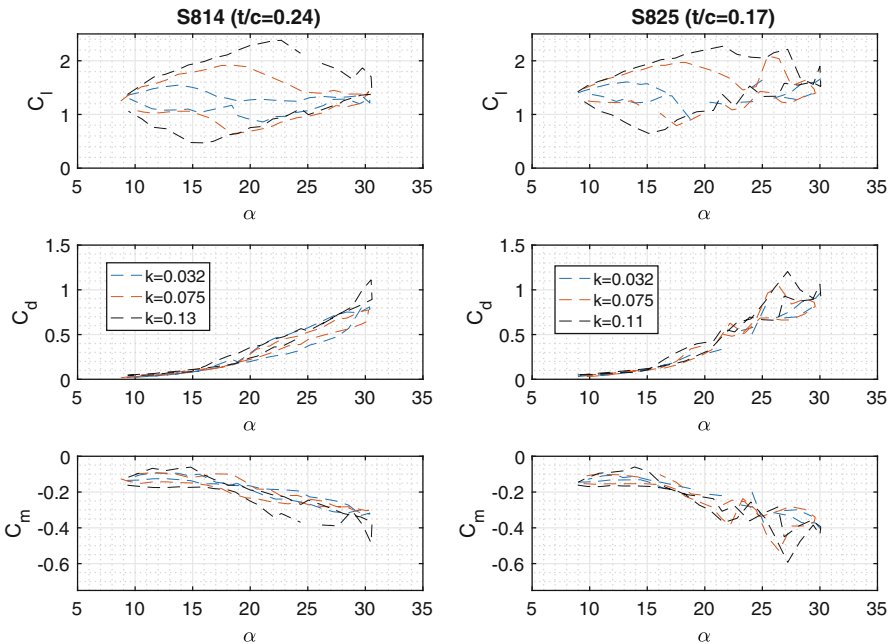


Fig. 2 OSU 2D C_l , C_d and C_m unsteady data (National Renewable Energy Laboratories) for the S814(left) and S825(right) airfoils, at different reduced frequencies

thinner section a pitching moment break (i.e. large $\frac{dC_m}{d\alpha}$) is present and leads to significant load fluctuations.

As highlighted before, the trends mentioned are valid in a two-dimensional configuration. In practice, for any real-life application and particularly for WE machines, there will be three-dimensional effects. The geometry of the lifting surface and particularly the shape of the wing or blade tip (Galbraith et al. 1996; Coton et al. 2001) will have an influence on the topology of the vortex structure and thus aerodynamic loading during DS events. In rotating blades, proximity to the tip (Wang et al. 2017) limits the maximum instantaneous C_l , C_d , and C_m values occurring over a cycle, and thus near the tip load hysteresis is decreased compared to mid-span stations. It is believed this effect is related with the finiteness of the wing/blade since towards the edge there is no physical barrier to sustain the lift-generation mechanism. As the pressure difference between the suction and pressure sides of the foil dwindles, the transient loads also decrease.

Dynamic Stall on Wind Energy Machines

The occurrence of DS on wind energy machines is naturally related with the time history of the AOA experienced at the blade sections. Referring back to blade element decomposition (**from figure in** ▶ Chap. 13, “Pragmatic Models: BEM with Engineering Add-Ons”), the AOA at each spanwise station depends on the rotational (Ω) and wind direction (U) velocity components, as well as local induction (a, a') and pitch setting (θ). For horizontal axis machines, this may be expressed by:

$$\alpha + \theta = \phi = \tan \frac{U(1 - a)}{\Omega r(1 + a')} \quad (2)$$

Given the typically large size and thus large inertia of modern WE machines, in normal operation rotational speed and pitch angle variations are slow ($\dot{\Omega} \approx \dot{\theta} \approx 0$) and thus do not usually bring about unsteady aerodynamic effects at the blade section level.

Variations in wind speed however may be ‘quick’ and thus directly play a role in the occurrence of DS on WE machines. The wind velocity will change in both space and time $U = f(x, y, z, t)$, and each blade section is swept across all azimuthal positions over each rotor revolution. As such, the AOA variations experienced by a blade section arise as a combination of both time variations of the local wind speed $\frac{\partial U(x_0, y_0, z_0, t)}{\partial t} \neq 0$ and rotational sampling (Connel 1982) of wind speed spatial gradients $U = f(x, y, z, t_0)$ over each revolution.

Dynamic Stall on HAWT

To assess the occurrence of DS on horizontal axis machines, it is common (Snel 2004) to approximate the effective velocity V from Expression 1 with the rotational

Table 1 Estimated 1P reduced frequencies along the span for the *NREL 5MW* machine

r/R	0.33	0.66	0.91
k	0.10	0.04	0.02

velocity component Ωr and thus obtain the reduced frequency:

$$k = \frac{\omega c}{2V} \approx \frac{\omega c}{2\Omega r} \approx \frac{f c}{2r} \quad (3)$$

where f is the non-dimensional frequency in Ps , ([► Chap. 10, “Dynamic Stall”](#)) so that is (Manwell et al. 2002) in multiples of the turbine rotor rotational frequency. Table 1 shows the values of reduced frequencies k considering a $f = 1$ P excitation for a ‘standard’ 5MW machine (Jonkman et al. 2009) obtained at different radial positions.

From Table 1, it is clear inboard stations ‘feel’ significant unsteady effects from a 1P excitation, and mid-span and even tip region sections may experience unsteady flow behaviour too. It is particularly relevant to consider 1P as the excitation frequency because both wind shear (Pereira et al. 2018) and yaw misalignment (Scheepers and Vermeer 1998) will result in a nearly harmonic AOA variation at a given blade section over each rotor revolution.

However, the 1P excitation is not the only frequency that may induce DS events on HAWT blades. Due to rotational sampling (Connel 1982), the spectrum of AOA fluctuations at the blade sections induced by atmospheric turbulence shows several peaks, at the 1P frequency and its multiples 2P, 3P, etc.. The effect of the turbine tower on the local wind speed (tower shadow) is felt once per blade per revolution, for both upwind and downwind rotor configurations. However, because the tower shadow is confined to rotor azimuth angles close to the vertically downward positions (Cermak and Horn 1968; Hibbs 1986), the blade section AOA spectrum exhibits higher harmonics than 1P.

Ultimately the occurrence of DS on HAWT blade sections depends not only on the wind field spatial and temporal variations but also on the HAWT structure and control strategy. Specifically, rotor blade deflections often bring about changes in AOA as discussed in ([► Chap. 15, “Aeroelastic Simulations Based on High-Fidelity CFD and CSD Models”](#)). Referring to figure [[figure in ► Chap. 13, “Pragmatic Models: BEM with Engineering Add-Ons”](#)], blade vibrations in the flapwise direction will induce apparent wind speed (U) variations and thus have a similar effect to a plunging or heaving airfoil. Blade edgewise deflections have much smaller magnitude (Jonkman et al. 2009) and are nearly aligned with the rotational speed component, and as such edgewise vibrations have a negligible contribution to AOA variations. Since the flapwise deflections will be larger for the outer stations of the blade, the time derivative of the apparent wind speed \dot{U} due to blade vibrations will also be larger towards the tip. Snel (Snel 2004) argues the combination of blade vibrations with the HAWT reduced frequency approximation from Eq. 3 produces unsteady effects that have approximately the same importance along the blade span.

Additionally one should consider that though root blade sections experience larger reduced frequencies, they are usually composed of thicker airfoil sections and are thus somewhat less prone to aerodynamic load hysteresis because the (static) stall is less abrupt than for thin airfoil sections owing to large LE radius. Moreover the phenomenon of rotational augmentation (Snel et al. 1993) will delay (static) stall to larger AOA and thus may also decrease the magnitude of the load hysteresis felt at inboard stations. This is further discussed in section “[Modelling Dynamic Stall in Wind Energy Machines](#)”.

All in all, the effective prediction of DS occurrence over HAWT blade sections and estimation of the associated loads on HAWTs can only be achieved if aero-servo-structural simulations (Rezaeiha et al. 2017b) are carried out, encompassing the different physical disciplines.

Dynamic Stall on VAWT

In vertical axis wind turbines, the plane in which the blade sections rotate coincides with the wind velocity vector \vec{U} , and as such the experienced AOA over each revolution is quite different from the HAWT case (► [Chap. 41, “Vertical-Axis Wind Turbine Aerodynamics”](#)). The approximation for effective velocity $V \approx \Omega r$ is often still valid for VAWT, meaning Expression 3 may be used to estimate the reduced frequency k for different excitation frequencies P . However, depending on the specific VAWT configuration, the distance between the blade section and the axis of rotation does not necessarily change along the blade span (e.g. for H-type machines it is constant), and as such the reduced frequency estimation presented above is not always relevant.

However, the phenomenon of DS is quite relevant for VAWT (Ferreira et al. 2009; Greenblatt et al. 2014) since there is a higher likelihood of occurrence than for HAWT. For typical VAWT applications, the tip-speed ratio is $\lambda \gg 1$, which means the AOA over a revolution may be approximated with:

$$\alpha = \frac{(1 - a) \cos \psi}{\lambda} \quad (4)$$

where ψ represents the azimuth angle. It is thus clear the experienced AOA may become very large, i.e. larger than the static stall angle, depending on the operational tip-speed ratio. This is in stark contrast with modern variable-pitch variable speed HAWT, which seldom experience AOA beyond the static stall angle during normal operation. As such, AOA fluctuations induced by atmospheric turbulence may produce DS events during VAWT normal operation.

Perhaps even more important than atmospheric turbulence, the impingement of shed vorticity on VAWT blades (Fujisawa and Shibuya 2001) may induce DS. Due to the geometric configuration of these machines, the azimuthally dependent AOA results in a continuously varying bound circulation and thus permanent

vortex shedding. The vortices released on the upstream half of the revolution (when $90 \text{ deg} < \psi < 270 \text{ deg}$ – ► [Chap. 41, “Vertical-Axis Wind Turbine Aerodynamics”](#)) are convected with the wind speed and may thus ‘hit’ the VAWT blades on the downstream half of the revolution, resulting in ‘quick’ fluctuations in AOA at the blade sections (McLaren 2011). As shown in Eq. 4 the operational AOA is largest at $270 \text{ deg} < \psi < 90 \text{ deg}$, i.e. on the downstream half of the revolution, and thus this vortex impingement often results in DS at the VAWT blade sections.

Unlike HAWT, wind shear and yaw misalignment are not expected to induce DS on VAWT blade sections; this is because for VAWT wind shear results in AOA variations along the span, not over each revolution, and obviously since VAWT are never misaligned with respect to the wind direction. Ultimately, and similarly to HAWT, accurate prediction of DS events and associated loads on VAWT requires dedicated aero-servo-structural computations, though the aerodynamics of VAWT is generally harder to simulate (Ferreira 2009).

Experimental Data on Dynamic Stall

The insight gained by the scientific community on the complex DS phenomena and its occurrence on WE machines has been achieved through decades of wind tunnel testing and data analysis. Experimental studies on dynamic stall date back to (at least) 1932 (Kramer 1932), with characterization of different physical quantities including balance measurements, surface pressure taps (Ramsay et al. 1995), smoke flow visualization (Galbraith et al. 1996) and flow field determination with particle image velocimetry (Ferreira et al. 2009).

Numerous experimental studies have been conducted to analyse the dynamic stall phenomenon in a two-dimensional configuration. This is both due to the relatively simple experimental apparatus required and because 2D performance may be (cautiously) used to (Guntur 2013) extrapolate towards actual 3D flow behaviour. Initially considered in the airplane wing context (Kramer 1932), dynamic stall in helicopter operation has received a lot of attention (Carr and Chandrasekhara 1996; Leishman and Beddoes 1986, 1989; Tran and Petot 1981) as it may occur during forward helicopter flight, i.e. in normal operation. From the early 1970s onwards, 2D experiments included a range of different tests on airfoils in pitching, heaving and ramp-up conditions, and a combination of surface pressure taps and flow visualization provided insight on the topology of the DS phenomenon, namely, on the formation, detachment and convection of LE vorticity. This knowledge was used to interpret load balance measurements and ultimately inspires many of the DS models proposed (Leishman and Beddoes 1989; Tran and Petot 1981; Gangwani 1984). Within the context of WE, dedicated dynamic stall experimental research started somewhat later, around the early 1990s. A few experimental studies tested the performance of specific WE airfoils under dynamic conditions, (Ramsay et al. 1995; Janiszewska et al. 1996; Fuglsang et al. 1998; Galbraith et al. 1992), which contributed to existing unsteady airfoil performance databases

(National Renewable Energy Laboratories; Gobbi 2010). The motivation for testing WE airfoils was that their geometry is somewhat different (thicker sections) from those used in helicopter blades, and as such the exact DS behaviour may differ too. Again, the remark is made here that the particular experimental conditions may reflect the specific quantities sought by a modelling philosophy and research group.

Several experimental efforts studying DS phenomena on rotating blades have been conducted (Boorsma et al. 2011; Hibbs 1986; Schreck et al. 2001). Such studies are significantly more challenging than two-dimensional configurations but provide much more insight on real HAWT performance, particularly on the actual occurrence and extent of DS when several effects are combined. Usually in HAWT wind tunnel tests DS is enforced by imposing a rather large yaw misalignment angle. This leads to large amplitude AOA variations at high reduced frequencies (Table 1) for the blade inboard sections, but obviously the DS events taking place under these conditions are also heavily influenced by the rotational augmentation (Guntur 2013). In order to gain insight on the overall flow topology, HAWT experiments aiming at studying DS may include pressure taps at different spanwise stations of the blade and also flow visualization.

A few studies have addressed DS on VAWT machines specifically (Fujisawa and Shibuya 2001; Paraschivoiu et al. 1988; Ferreira et al. 2009) and have, namely, investigated the influence of blade tip geometry, aspect ratio and tip-speed ratio on the DS characteristics of vertical axis machines (Fig. 3).

Dynamic Stall Modelling

From the previous sections, it is clear DS encompasses a complex set of interlinked phenomena, all the more in rotating, wind energy machines where aerodynamic effects, such as rotational augmentation (Guntur 2013) and tip vortex interactions (Paraschivoiu et al. 1988), come together with blade structural vibrations. In short, modelling DS effects in WE machines is not straightforward at all. As hinted throughout the previous sections, aerodynamicists, particularly people involved in helicopter and later WE machine's design and analysis, have been working on the topic(s) for a few decades (Gangwani 1984; Leishman and Beddoes 1989; Sheng et al. 2008).

Different types of DS modelling have been used, ranging from simple, purely empirical approaches, i.e. curve fitting of experimental data, to complex computational fluid dynamics (CFD) simulations. Though generally speaking more complex methods will capture more of the DS phenomena physics and thus yield more accurate predictions, it is noted proper CFD simulations can only be obtained using the Navier-Stokes equations with a suitable turbulence model, given the nature of the interacting phenomena, and even then it is not clear whether URANS simulations (Guilmineau and Queutey 1999) always outperform simpler methods compared to experimental data.

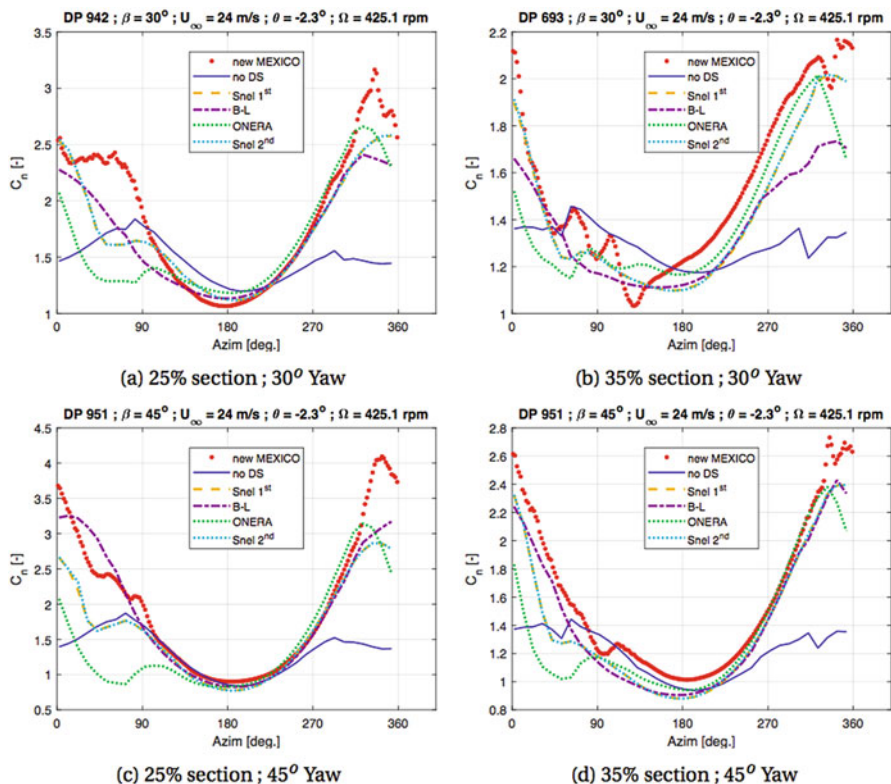


Fig. 3 Normal force coefficient variation with azimuth angle for HAWTs in yawed flow conditions – simulated from different dynamic stall models (Snel 1997; Tran and Petot 1981; Leishman and Beddoes 1989) and compared with New MEXICO measurements, for different spanwise locations and yaw misalignment angles. (Adapted from Khan 2018)

Beddoes-Leishman Type of Dynamic Stall Modelling

In practice, the compromise between computational effort and required accuracy of DS modelling usually leads to the employment of the so-called semi-empirical methodologies. Such approaches do model the main physical phenomena associated with dynamic stall but rely on experimental data to tune the specific values of the modelling parameters. Additionally, the ease of implementation of semi-empirical methods in aeroelastic WE codes (Jonkman et al. 2021; Rezaeiha et al. 2017b) simulating WE machines using BEM theory has greatly contributed to the dissemination of such DS models.

Several semi-empirical models developed specifically with wind energy applications in mind have been proposed (Snel 1997; Øye 1990; Sheng et al. 2008), though models originally developed for helicopter rotors (Tran and Petot 1981; Leishman and Beddoes 1989) are also commonly used for estimation of loads on

WE machines. Due to its very extensive employment (Gonzalez and Munduate 2007; Jonkman et al. 2021), dedicated subsequent model refinement studies (Mert 1999), good agreement with experimental data and relative simplicity, we will now focus on the Beddoes-Leishman (Leishman and Beddoes 1989) dynamic stall model. For further information and a more detailed overview of existing DS models, the reader is referred to Pereira (2010) and Khan (2018).

The Beddoes-Leishman method is capable of assessing the unsteady lift, pitching moment and drag, and it is characterized by having a rather complete physical representation of the unsteady aerodynamic problem. It is composed of three subsystems, briefly explained here for the **normal** force coefficient (C_N):

1 – An attached flow module for the unsteady linear aerodynamic loads, which considers both the circulatory (C_N^C) (Theodorsen 1935) and impulsive (Fung 1993) (C_N^I) components. At instant n the circulatory component is obtained by computing an equivalent AOA ($\alpha_{Eq,n}$) and using indicial (or deficiency) functions (X_n, Y_n). The impulsive component is typically significantly smaller for WE machine operation, and it is thus sometimes neglected (Barlas 2011) in wind turbine aerodynamic modelling. The total, instantaneous attached flow normal force coefficient ($C_{N,n}^P$) is simply the sum of both circulatory and impulsive components.

$$C_{N,n}^C = C_{N\alpha} \alpha_{Eq,n} = C_{N\alpha} (\alpha_n - X_n - Y_n) \quad (5)$$

$$X_n = X_{n-1} e^{-b_1 \Delta S} + A_1 \Delta \alpha_n e^{-b_1 \frac{\Delta S}{2}} \quad (6)$$

$$C_{N,n}^P = C_{N,n}^C + C_{N,n}^I \quad (7)$$

where b_1 and A_1 are constants fit to the linear range (attached flow) experimental airfoil performance and Y_n is defined analogously to X_n . ΔS represents the distance (in semi-chords) travelled by the airfoil over two consecutive instants ($n, n - 1$).

2 – A separated flow module for the nonlinear aerodynamic loads, which uses Kirchhoff/Helmholtz (reviewed in Thwaites (1961)) static trailing edge separation chordwise position $f(\alpha)$ and the angle of attack history to calculate the instantaneous flow separation point (f'') and the associated (viscous) aerodynamic force coefficient C_N^f .

$$C_N = C_{N\alpha} \left(\frac{1 + \sqrt{f''}}{2} \right)^2 \quad (8)$$

where $C_{N\alpha}$ is the slope of the (steady) normal coefficient experimental data. Since there is a lag in the leading edge pressure response with respect to the attached flow module, an intermediate normal force coefficient $C'_{N,n}$ is calculated with:

$$C'_{N,n} = C_{N,n} - D_{P,n} \quad (9)$$

from this intermediate normal force coefficient, a new effective AOA is calculated with:

$$\alpha_{f,n} = \frac{C'_{N,n} - C_{N_0}}{C_{N_\alpha}} \quad (10)$$

where C_{N_0} is the (static) normal force coefficient at zero incidence. From this effective AOA $\alpha_{f,n}$, the instantaneous chordwise separation point is finally calculated by applying another deficiency function to account for the lag in the response of the boundary layer:

$$f''_n = f'_n - D_{f,n} \quad (11)$$

where deficiency function $D_{f,n}$ depends on the empirically derived (viscous) time constant T_f . Finally the effective chordwise separation point is used in Eq. 8 to compute the instantaneous (viscous) normal force coefficient C^f_N at instant n according to:

$$C^f_{N,n} = C_{N_\alpha} \left(\frac{1 + \sqrt{f''_n}}{2} \right)^2 \alpha_{Eq,n} + C^I_{N,n} \quad (12)$$

3 – A dynamic stall module for the aerodynamic loads induced by the leading edge vortex, which simulates the LE concentrated vorticity build-up, detachment and convection across the airfoil's upper surface and into the wake. The LE vortex detachment event is determined by comparison with a critical condition (typically based on equivalent LE pressure (Leishman and Beddoes 1989) or maximum normal force coefficient Pereira et al. 2012), whereas the actual vortex contribution C^V_N to the instantaneous airfoil loads is estimated using the vortex travel time τ^V . As long as the vortex is situated over the airfoil, the normal force coefficient will increase, and this increment is estimated with:

$$C_{V,n} = C^C_{N,n} \left(1 - \frac{1 + \sqrt{f''_n}}{4} \right) \quad (13)$$

The total vortex contribution at instant n is calculated with:

$$C^V_{N,n} = C^V_{N,n-1} e^{-\frac{\Delta S}{T_V}} + (C_{V,n} - C_{V,n-1}) \frac{-\Delta S}{2T_V} \quad (14)$$

where T_V is the empirical constant that regulates the vortex contribution's decay. The total, instantaneous normal force coefficient $C_{N,n}$ is then finally computed with:

$$C_{N,n} = C^f_{N,n} + C^V_{N,n} \quad (15)$$

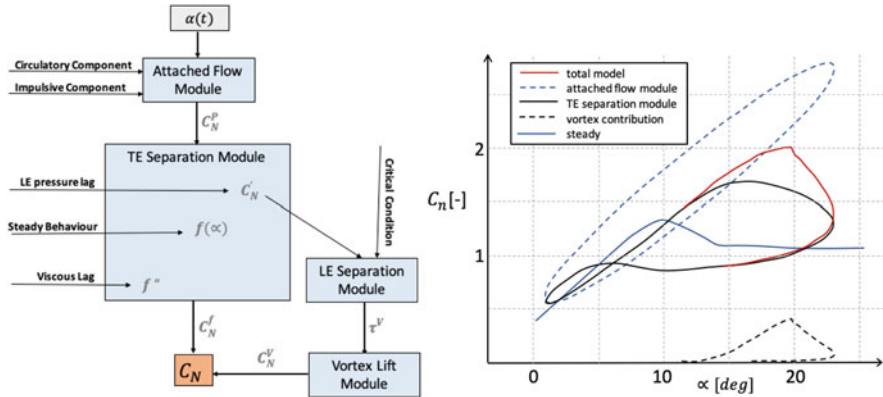


Fig. 4 *left* – Flowchart of Beddoes-Leishman type of dynamic stall models and *right* – decomposition of Beddoes-Leishman model showing the contribution of each module component. (Adapted from Pereira et al. 2012)

From the expressions shown above, it is clear that the so-called time constants (T_P, T_f, T_V) have a major role in the instantaneous aerodynamic forces. For a discussion on typical values for these constants, the reader is referred to Mert (1999) and Pereira et al. (2012).

The equations displayed above are used to estimate the normal force coefficient. The instantaneous **tangential** force coefficient $C_{C,n}$, i.e. along the chordwise direction, is estimated with:

$$C_{C,n} = \eta C_{N_\alpha} \alpha^2 E_{q,n} \sqrt{f''_n} \tag{16}$$

where η represents the so-called recovery factor, which is introduced because the airfoil does not realize 100% of the chordwise force attained in potential flow. This factor is also obtained empirically and has a typical value $\eta \approx 0.95$.

Figure 4 illustrates the different modules that comprise the Beddoes-Leishman type of modelling approach and main variables used in the computation of instantaneous loads, together with a graphical representation of the contribution of each module to the total loads experienced.

Like any physical model, the Beddoes-Leishman method does have limitations; for example, typically in the implementation of this model, only one LE-originated vortex structure is considered simultaneously, and the contribution of the LE vortex is neglected when it is convected ‘far enough’ from the airfoil. However, when very high reduced frequencies are considered, multiple LE vortex structures may be present, which can lead to abrupt load variations, particularly ‘spikes’ in the lift coefficient as observed in the experimental results from Fig. 2 around the

maximum AOA. To accurately capture such secondary vortex structures, specific delayed detached eddy simulation approaches may be used (Guntur et al. 2015).

Within semi-empirical, engineering DS models, and as hinted before, more complex Beddoes-Leishman type of approaches have been proposed, which can yield better agreement with experimental data. Such methods (Sheng et al. 2008; Tran and Petot 1981) however typically require a very significant number of experimental parameter values (around 20 whereas the Beddoes-Leishman uses only 4) derived under 2D conditions, which are specific to each airfoil section geometry and unsteady forcing condition. This may become slightly impractical and, in this author's opinion, somewhat defeats the purpose of employing engineering models. Additionally, and as mentioned before, DS in WE machines is never strictly a 2D aerodynamic event, and the coupling of different phenomena may have a larger influence (Guntur et al. 2015) than specific improvements of accuracy in 2D configurations bring.

Modelling Dynamic Stall in Wind Energy Machines

Since DS models are typically derived and/or tuned to match 2D experimental (airfoil section) data, one must be careful when attempting to model actual WE machines' observed behaviour.

As hinted before, one of the main 'culprits' for DS occurrence on **HAWT** is yaw misalignment, particularly for inboard sections. At blade stations close to the root, however, there will also be 'static' stall delay. Several models for the so-called rotational augmentation have been proposed (Snel et al. 1993; Chaviaropoulos and Hansen 2000), which typically correct the airfoil section 2D polar based on the local chord-to-blade-radius ratio, in practice prolonging the linear portion of the lift curve to larger AOA. Such a correction however means the maximum (static) lift C_l and normal C_n force coefficients will be increased. Since typically the sectional rotationally augmented static polar is used as input to semi-empirical DS models (Jonkman et al. 2021; Guntur 2013), the instantaneous load estimation will be directly affected. The maximum sectional (static) C_n is associated with the magnitude of LE suction peak and extent of the separated flow region, and is often used (in some form) as the criterion (Pereira et al. 2012; Khan 2018) for LE vortex detachment in dynamic conditions, and thus essentially controls the contribution of LE shed vorticity to the total instantaneous load experienced.

In addition to the maximum (static) lift or normal force coefficient, the fact that blades are rotating may affect the dynamics of trailing edge flow separation as well. Due to the radial pressure gradient, blade spanwise flow component and associated Coriolis force, the effective time necessary for the flow and specifically TE separation location (f) to adapt to, e.g. variations in AOA is changed with respect to a 2D, non-rotating scenario. In terms of DS modelling, this might require an adaptation of the time constants (Mert 1999) controlling the TE separation

point evolution. This aspect is particularly relevant for smart rotor (► [Chap. 6 “Blade Design with Passive Flow Control Technologies”](#)) applications which typically rely on TE flaps to control the flow and thus regulate (Barlas 2011; Bergami 2014) the blade-integrated aerodynamic loads.

It must be noted that although rotational augmentation and dynamic stall are quite different physical phenomena which obviously have a complex interaction, typically simple model superposition is used. Nevertheless, reasonable agreement (Guntur et al. 2015; Pereira et al. 2012; Khan 2018) is usually obtained, at least in terms of the sectional load amplitude over a rotor revolution, as illustrated in Fig. 3.

As for DS modelling on VAWTs, and since the topology of such machines does not easily lend itself to accurate BEM variant formulations, semi-empirical methods are perhaps employed more seldom than for horizontal machines. Instead, often CFD approaches (Rezaeiha et al. 2017a; Almohammadi et al. 2015) are used to estimate the instantaneous aerodynamic loading, which precludes the need for engineering DS methods. Nevertheless, specific studies have recently been published in which the Beddoes-Leishman model is adapted to the VAWT environment and coupled to a BEM formulation (Pirrung and Gaunaa 2018). Earlier studies also tested different semi-empirical DS models (Cardona 1984) in free-vortex VAWT aerodynamics’ formulation, in which the relevance of including flow curvature (Migliore et al. 1980) to accurately capture the instantaneous loads in vertical axis machines was highlighted.

As mentioned before, DS models usually rely on the C_l , C_d and C_m polars, obtained under static conditions. However, even under static conditions, there will be stall hysteresis (Timmer 2008), meaning that around the stall AOA the value of the (steady) lift coefficient will depend on whether the AOA is increasing or decreasing. For practical purposes, particularly when simulating the loads on WT blades, it is recommended to use the upper branch of the lift and drag polars as input to DS models, since otherwise the instantaneous aerodynamic loads will be underestimated.

A final remark is made on the influence of the surface roughness and its impact on DS modelling. As mentioned before, real operating conditions are often emulated by imposing transition on the LE, and this ‘rough’ configuration will lead to a smaller maximum static C_l than ‘clean’ conditions. As DS models often use the maximum static lift coefficient to define the onset of LE vortex shedding, it is clear that having ‘rough’ instead of ‘clean’ conditions will have a significant impact on the load amplitude (Bousman 2000) occurring during DS phenomena. It is again noted however that the load dynamics, which is the delay in the unsteady loading with respect to the instantaneous AOA, seems to be relatively insensitive to LE transition.

Cross-References

- [Pragmatic Models: BEM with Engineering Add-Ons](#)
- [Vertical-Axis Wind Turbine Aerodynamics](#)

References

- Almohammadi KM, Ingham DB, Ma L, Pourkashanian M (2015) Modeling dynamic stall of a straight blade vertical axis wind turbine. *J Fluids Struct* 57:144–158
- Barlas T (2011) Active aerodynamic load control on wind turbines: aeroservoelastic modeling and wind tunnel experiments. Ph.D. Dissertation, TUDelft
- Bergami L (2014) Smart rotor modelling – aero-servo-elastic modeling of a smartRotor with adaptive trailing edge flaps. Springer
- Bertagnolio F, Sorensen N, Johansen J, Fuglsang P (2001) Wind turbine airfoil catalogue – R-1280. Risø, Technical Report
- Boorsma K, Schepers JG et al (2011) Final report of IEA task 29, Mexnext (phase 1), analysis of Mexico wind tunnel measurements. ECN-E-12-004, Energy Research Center of the Netherlands
- Bousman G (2000) Airfoil dynamic stall and rotorcraft maneuverability. NASA/TM-2000-209601
- Cardona JL (1984) Flow curvature and dynamic stall simulated with an aerodynamic free-vortex model for vawt. *Wind Eng* 8(3):135–143
- Carr LW, Chandrasekhara MS (1996) Compressibility effects on dynamic stall. *Prog Aerosp Sci* 32(6):523–573
- Cermak JE, Horn JD (1968) Tower shadow effect. *J Geophys Res* 73:1869–1876
- Chaviaropoulos P, Hansen M (2000) Investigating three-dimensional and rotational effects on wind turbine blades by means of a quasi-3D Navier-Stokes solver. *J Fluids Eng* 122:330–336
- Connel JR (1982) The spectrum of wind speed fluctuations encountered by a rotating blade of a wind energy conversion system. *J Solar Energy* 29(5):363–375
- Coton FN, McD Galbraith RA, Green RB (2001) The effect of wing planform shape on dynamic stall. *Aeronaut J* 105(1045):151–159
- Daley DC, Jumper EJ (1984) Experimental investigation of dynamic stall for a pitching airfoil. *J Aircr* 21(10):831–832
- Ferreira CS (2009) The near wake of the VAWT: 2D and 3D views of the VAWT aerodynamics. TUDelft Ph.D. Thesis
- Ferreira C, van Kuik G, van Bussel G, Scarano F (2009) Visualization by PIV of dynamic stall on a vertical axis wind turbine. *Exp Fluids* 46(1):97–108
- Fuglsang P, Antoniou P, Bak C, Madsen H (1998) Wind tunnel test of the RISOE-1 airfoil. Risoe-R999(EN)
- Fujisawa N, Shibuya S (2001) Observations of dynamic stall on darrieus wind turbine blades. *J Wind Eng Indus Aerodyn* 89:201–214
- Fung YC (1993) An introduction to the theory of aeroelasticity. Dover Phoenix Editions, pp407
- Galbraith RAM, Coton FN, Jiang D, Gilmour R (1992) Summary of pressure data for thirteen airfoils on the university of glasgow airfoil database. Glasgow University Report 9221
- Galbraith RAM, Coton FN, Jiang D, Gilmour R (1996) The dynamic stalling characteristics of a rectangular wing with swept tips. In: Proceedings Conference 22nd European Rotorcraft Forum
- Gangwani S (1984) Synthesized airfoil data method for prediction of dynamic stall and unsteady airloads. *Vertica* 8:93–118
- Gobbi G (2010) Analysis and reconstruction of dynamic-stall data from nominally two-dimensional aerofoil tests in two different wind tunnels. Ph.D. Thesis – University of Glasgow
- Gonzalez A, Munduate X (2007) Unsteady modelling of the oscillating S809 aerofoil and NREL phase VI parked blade using the Beddoes-Leishman dynamic stall model. *J Phys Conf Ser* 75(1):012020
- Greenblatt D, Ben-Harav A, Mueller-Vahl H (2014) Dynamic stall control on a vertical-axis wind turbine using plasma actuators. *AIAA J* 52(2):456–462
- Guilmineau E, Queutey P (1999) Numerical study of dynamic stall on several airfoils sections. *AIAA J* 37:128–130
- Guntur S (2013) A detailed study of the rotational augmentation and dynamic stall phenomena for wind turbines. DTU Ph.D. Dissertation
- Guntur S, Schreck S, Sørensen N, Bergami L (2015) Modeling dynamic stall on wind turbine blades under rotationally augmented flow fields. NREL Technical Report – TP-5000-63925

- Hibbs BD (1986) Hawt performance with dynamic stall. Technical Report SERI/STR-217-2732
- Janiszewska JM, Ramsay RR, Hoffmann MJ, Gregorek GM (1996) Effects of grit roughness and pitch oscillations on the S814 airfoil. NREL/TP-442-8161
- Jonkman J, Butterfield S, Musial W, Scott G (2009) Definition of a 5-MW reference wind turbine for offshore system development. NREL-TP500-38060
- Jonkman J et al (2021) NWTC information portal (fast). <https://nwtc.nrel.gov/FAST>
- Khan M (2018) Dynamic stall modelling for wind turbines. Master Thesis – TUDelft
- Kramer M (1932) Increase in the maximum lift of an airplane wing due to a sudden increase in its effective angle of attack resulting from a gust. NACA Technical Memorandum No. 678
- Leishman J (2002) Challenges in modeling the unsteady aerodynamics of wind turbines. In: 21st ASME Wind Energy Symposium, Reno
- Leishman J (2006) Principles of helicopter aerodynamics. Cambridge aerospace series. Cambridge University Press
- Leishman J, Beddoes T (1986) A generalised model for airfoil unsteady aerodynamic behaviour and dynamic stall using the indicial method. In: 42nd Annual Forum of the American Helicopter Society
- Leishman J, Beddoes T (1989) A semi-empirical model for dynamic stall. J Am Helicopter Soc 34:3–17
- Lorber PF, Carta FO (1987) Airfoil dynamic stall at constant pitch rate and high reynolds number. In: AIAA 19th Fluid Dynamics, Plasma Dynamics and Lasers Conference, vol 1329
- Magnan A (1934) Le Vol des Insectes. Hermann, Paris
- Manwell J, McGowan J, Rogers A (2002) Wind energy explained-theory, design and application. Wiley, Chichester
- McLaren KW (2011) A numerical and experimental study of unsteady loading of high solidity vertical axis wind turbines. McMaster University – Ph.D. Thesis
- Mert M (1999) Optimization of semi-empirical parameters in the FFA-beddoes dynamic stall model. FFA TN 1999-37
- Migliore PG, Wolfe WP, Fanucci JB (1980) Flow curvature effects on darrieus turbine blade aerodynamics. J Energy 4:2(3):49–55
- National Renewable Energy Laboratories Unsteady airfoil Ohio state university data. Available at https://wind.nrel.gov/airfoils/OSU_data/data/
- Øye S (1990) Dynamic stall simulated as time lag of separation. In: Proceedings of the Fourth IEA Symposium on the Aerodynamics of Wind Turbines, Rome, 20–21 Nov
- Paraschivoiu I, Desy P, Masson C (1988) Blade tip, finite aspect ratio, and dynamic stall effects on the darrieus rotor. J Propuls Power 4(1):73–80
- Pereira R (2010) Validating the Beddoes Leishman dynamic stall model in the horizontal axis wind turbines environment. TUDelft Master Thesis
- Pereira R, van Bussel GJW, Timmer WA (2012) Active stall control for large offshore horizontal axis wind turbines; a conceptual study considering different actuation methods. IOP – Science of Making Torque
- Pereira R, de Oliveira G, Timmer WA, Quaegebeur E (2018) Probabilistic design of airfoils for horizontal axis wind turbines. J Phys Conf Ser 1037(2):022042
- Pereira R, Schepers G, Pavel Marilena D (2012) Validation of the Beddoes Leishman dynamic stall model for horizontal axis wind turbines using Mexico data. Wind Energy 16(2):207–219
- Pirrung G, Gaunaa M (2018) Dynamic stall model modifications to improve the modeling of vertical axis wind turbines. DTU Wind Energy E
- Ramsay RF, Hoffman MJ, Gregorek GM (1995) Effects of grit roughness and pitch oscillations on the S809 airfoil. NREL/TP-442-7817, 12
- Rezaeiha A, Kalman I, Blocken B (2017a) Effect of pitch angle on power performance and aerodynamics of a vertical axis wind turbine. Appl Energy 197:132–150
- Rezaeiha A, Pereira R, Kotsonis M (2017b) Fluctuations of angle of attack and lift coefficient and the resultant fatigue loads for a large horizontal axis wind turbine. Renew Energy 114:904–916
- Schepers JG, Vermeer L (1998) EEN engineering model voor scheefstand op basis van windtunnelmetingen. ECN-CX-98-070

- Schreck S, Robinson MC, Hand MM, Simms D (2001) Blade dynamic stall vortex kinematics for a horizontal axis wind turbine in Yawed conditions. *J Solar Energy Eng Trans Asme* 123:272–281
- Seto LY, Galbraith RA (1985) The effect of pitch rate on the dynamic stall of a NACA 23012 aerofoil. In: 11th European Rotorcraft Forum, London: Paper No 34, September 1985
- Sheng W, Galbraith RAM, Coton FN (2006) A new stall onset criterion for low speed dynamic stall. *J Solar Energy Eng* 128(4):461–471
- Sheng W, Galbraith R, Coton F (2008) A modified dynamic stall model for low mach numbers. *J Solar Eng* 130:031013–1/031013–10
- Snel H (1997) Heuristic modelling of dynamic stall characteristics. In: Conference Proceedings European Wind Energy Conference, pp 429–433
- Snel H (2004) Application of a modified theodorsen model to the estimation of aerodynamic forces and aeroelastic stability. In: Conference Proceedings European Wind Energy Conference, pages ECN–RX–04–120
- Snel H, Houwink R, van Bussel GJW, Bruining A (1993) Sectional prediction of 3D effects for stalled flow on rotating blades and comparison with measurements. In: Proceedings of the European Community Wind Energy Conference, pp 395–399
- Theodorsen T (1935) General theory of aerodynamic instability and the mechanism of flutter. NACA, Report 496
- Thwaites B (1961) *Incompressible aerodynamics*. Cambridge University Press, Cambridge
- Timmer WA (2008) Two-dimensional low reynolds number wind tunnel results for airfoil NACA0018. *Wind Eng* 32(6):525–537
- Timmer WA (2009) An overview of NACA 6-digit airfoil series characteristics with reference to airfoils for large wind turbine blades. In: 47th AIAA Aerospace Sciences Meeting, p 268
- Timmer WA, van Rooij RPJOM (2003) Summary of the Delft university wind turbine dedicated airfoils. AIAA AIAA-2003–0352
- Tran CT, Petot D (1981) Semi-empirical model for the dynamic stall of airfoils in view of the application to the calculation of responses of a helicopter in forward flight. *Vertica* 5(1):35–53
- Wang Q, Zhao Q, Yin J, Wang B (2017) Three-dimensional effects on dynamic stall of rotor airfoil. In: American Helicopter Society 73rd Annual Forum